Mine Water and the Environment (2020) 39:121–134
https://doi.org/10.1007/s10230-019-00649-7

TECHNICAL ARTICLE

Impacts of Aquitard Properties on an Overlying Unconsolidated Aquifer in a Mining Area of the Loess Plateau: Case Study of the Changcun Colliery, Shanxi

Shuyuan Xu[1] · Yongbo Zhang[1] · Hong Shi[2] · Zhixiang Zhang[1,3] · Junfeng Chen[1]

Received: 1 March 2019 / Accepted: 16 December 2019 / Published online: 1 January 2020

Abstract
Quaternary unconsolidated porous aquifers are crucial to industrial, agricultural, and domestic water as well as ecological requirements in semiarid regions. Underground mining can influence aquifers even when they are located out of the fractured zone. Slight but continuous leakage should not be ignored. This study focused on the flow from a leaky aquifer. The deformation and fissure distribution characteristics and changes in the water resistance of a clay aquitard underlying an unconsolidated aquifer were studied by physical modeling, and the impacts on the unconsolidated aquifer were analyzed. Considering the mining-induced changes in the overburden hydraulic conductivity, we used numerical groundwater flow simulations of an unconsolidated aquifer to predict the flow dynamics of the aquifer for different scenarios. The influences of aquitard thickness and permeability on the groundwater flow regime of the regional unconsolidated aquifer under the mining area were quantitatively analyzed. This case study shows that the degree of coal extraction influence on the leaky confined aquifer depends on the properties of the aquitard beneath the aquifer. When the thickness was as high as 40 m and the hydraulic conductivity was as low as 10^{-6} cm/s, the aquitard could effectively prevent a water level depression. The results have practical implications for coal mining with water resource conservation.

Keywords Aquitard thickness · Hydraulic conductivity · Numerical simulation · Physical modeling · Water conservation mining

Electronic supplementary material The online version of this article (https://doi.org/10.1007/s10230-019-00649-7) contains supplementary material, which is available to authorized users.

✉ Yongbo Zhang
zfstzhang@sina.com

Shuyuan Xu
xsyuan1981@126.com

Hong Shi
sx_hosh196@sina.com

Zhixiang Zhang
zhangzhixiang@tyut.edu.cn

Junfeng Chen
chenjunfeng@tyut.edu.cn

1 College of Water Resources Science and Engineering, Taiyuan University of Technology, Taiyuan 030024, China

2 College of Environmental Science and Engineering, Taiyuan University of Technology, Taiyuan 030024, China

3 Department of Earth Sciences, University of the Western Cape, Cape Town 7535, South Africa

Introduction

Being a coal resource area, Shanxi is an important base of countrywide energy for the heavy chemical industry. The coal resources are characterized by rich reserves, a wide distribution, multiple types, good quality, and easy exploitation. The reserves in Shanxi account for one third of the country's total, and the output has accounted for a quarter of China's total for the last few decades. In addition, Shanxi is located on the Loess Plateau, the world's largest loess accumulative area, which is a typical arid and semiarid region in northern China with low rainfall, high evaporation and a weak ecological environment. In this region, due to the limited availability of surface water systems, the groundwater in the Quaternary unconsolidated aquifers is the primary resource for national economic development, residents' livelihoods, and ecoenvironmental maintenance (Scanlon et al. 2010; Yang et al. 2001). However, extensive and intensive exploitation activities over many decades have resulted in alarming situations in terms of ecological conditions and domestic water availability (Booth 2006; Xie et al. 2018). Some unconsolidated aquifers are being rapidly depleted by underground mining (Newman et al. 2017). Since the growth of land vegetation is closely associated with the groundwater depth, the declining groundwater levels have resulted in surface ecological environmental deterioration (Brandyk et al. 2016; Kloosterman et al. 1995). Inhabitants of the area are facing a severe shortage of water for daily living.

Additionally, coal bases around the world have suffered considerable water resource shortages, water contamination, and water disputes due to the destruction of groundwater resources during construction and development (Booth 2006). The damage to groundwater has become a bottleneck problem that prevents mining areas from attaining sustainable economic development. Therefore, groundwater should be treated as a precious resource rather than as a hazard (Hill and Price 1983; Ma et al. 2015). To promote sustainable development and ecoenvironmental rehabilitation, the problem demanding prompt solutions is how to reduce or avoid the damage from underground mining to overlying unconsolidated aquifers. To this end, “coal mining with water resource conservation” and “Green Mining” were proposed in China (Bian et al. 2012; Ma et al. 2015; Zhang et al. 2011).

Underground mining results in the movement and failure of overburden strata (Peng 1992; Singh and Kendorski 1981), and the integrity and permeability of overlying aquifers is affected to varying degrees (Karacan and Goodman 2009; Liu et al. 1997; Tammetta 2015). Mining disturbances have disrupted recharge-discharge balances and altered water flow paths (Kloosterman et al. 1995; Zhang et al. 2018). In some deep coalfields, even if excavation does not cause groundwater from an unconsolidated aquifer to gush out, it can lead to continual and slow drawdown, which ultimately causes ecological damage.

The intermediate zones in the overburden play a critical role in water protection (Singh and Kendorski 1981). To avoid damaging aquifers with water supplies, an aquifer protection mining technique has been applied in mining areas of northwestern China. In this approach, aquitard stability research is the core of ground control (Huang 2014). Therefore, to coordinate coal extraction, water conservation and supergene ecoenvironmental protection, it is essential to have a more comprehensive understanding of how underground mining affects overlying unconsolidated aquifers and to characterize the flow field at different aquitard parameters under mining conditions, which may provide guidance for water level recovery.

Earlier studies on the impacts of underground mining were more about water inrush, overburden failure, ground subsidence and groundwater depletion (e.g. Wang and Li 1987; Zeng et al. 2018). Analyses and studies of the mechanisms of the extraction effects on aquifers and groundwater have been conducted by a few researchers (Booth 2006; Newman et al. 2017). These studies focused mostly on the fractured zone owing to its connectivity with goafs (Du and Gao 2017; Miao et al. 2011; Zhang et al. 2017), and the target aquifers from both security and environmental perspectives were inside the damaged zone, where groundwater can flow directly into the mine pits through fractures. However, the water table depression caused by leakage was often neglected. In addition, there were no quantitative analysis on the correlation between aquitard properties and the flow field of unconsolidated aquifers. In recent years, numerical simulations have been widely used for mine water disaster prevention and water resource management (Ben-Itzhak and Gvirtzman 2005; Izady et al. 2017; Qiu et al. 2015; Sun et al. 2015; Yuan et al. 2009), flow models have rarely considered changes in the permeability of the rock overlying the mine to predict the hydrodynamics of aquifers.

The purpose of this study was to analyze the characteristics and mechanism of aquifer failure by physical modeling and to discuss the groundwater level response to overburden failure. An attempt has been made in this study to establish a three-dimensional groundwater flow model and quantitatively analyze the impacts of variable aquitard properties on an unconsolidated aquifer and its flow field in a coal extraction area. The results may provide a theoretical basis for “water conservation mining” and regional sustainable development planning in the semiarid Chinese Loess Plateau region.

Research Area

In this study, the mining area (termed S6) of the Changcun coal mine was used to analyze the impacts of an aquitard on the overlying unconsolidated aquifer after mining. Its geological and hydrogeological setting is similar to those of most areas with thick loess deposits. The area is representative of most regions that face groundwater decreases, increasing water shortages, and severe constraints on domestic water and agricultural production.

Location of Study Area

The Changcun Colliery is an extremely large modern mine in Shanxi Province. It is located within the Shangdang Basin in the just eastern part of the Loess Plateau and covers an area of 107.38 km^2 (Fig. 1). It is a semiarid zone with an average annual rainfall of 550 mm and an average annual evaporation of 1739 mm. Mining area S6 is located in the southeast of the mine, with an area of 6.34 km^2. Fully mechanized longwall mining without backfilling is performed, and its service time is ≈ 5 years.

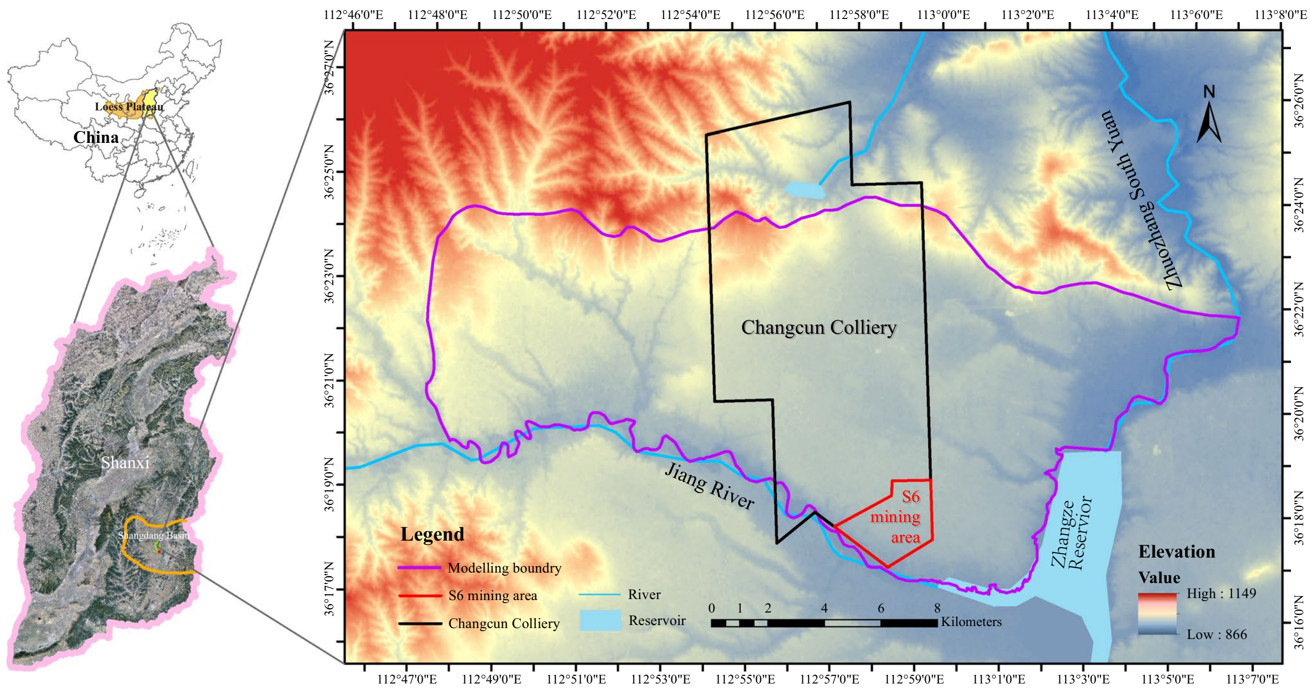

Fig. 1 Location of the study area

Geological and Hydrogeological Settings

The coal mine is widely covered by Quaternary loess, and the area has a gently rolling topography. Coal seam no. 3 in the Lower Permian Shanxi Formation is currently the main unit mined, and it is nearly horizontal, with an average depth of ≈ 300 m.

The aquifer system above the coal seam contains an unconsolidated porous aquifer, a weathered aquifer, and fractured rock aquifers. The Quaternary unconsolidated aquifer, with a water yield of 1.31–16.66 L/(s m), actually consists of two aquifers. The first, which is generally phreatic, is Middle Pleistocene in age and is only ≈ 2 m thick, with a low water yield. The water table is ≈ 5 to 10 m below the ground level, and is obviously affected by precipitation. The second aquifer is confined and located in the Lower Pleistocene strata, with a thickness of 36–60 m. This aquifer has a water level of + 927.29 to + 943.74 m and is enclosed by a silty clay layer with a hydraulic conductivity of 7.39×10^{-5} cm/s, which largely isolates the aquifer from lower strata. According to Tunliu County Annals, the shallow groundwater levels declined by an average of 4.87 m from 2006 to 2015, with an annual average decline of 0.49 m. The average annual recharge was 108 million m^3 during the same period, and this water supply is essential to those living and working in the area.

Both the weathered and fractured rock aquifers have poor water yields. The 50 m thick weathered aquifer has a water level of + 943.13 m, and its specific yield is 0.046–0.086 L/(s m). The fractured rock aquifers above the coal seam are composed mainly of multilayer coarse- and fine-grained sandstones, in which the water-bearing space is dominated by sandstone fractures. This aquifer has a water level of + 864.92 to + 914.52 m, and its specific yield is 0.0556–0.253 L/(s m).

The stratigraphic lithology and mechanical properties are shown in Fig. 2. The loess cover is 108 m thick, and the available aquifer and aquitard at the base are ≈ 44 m and 20 m, respectively.

Materials and Methods

Physical Modeling

Experimental Apparatus and Materials

The mining model used panel S6–9 in the S6 mining area as the geological prototype. The mold frame was 430 cm long, 40 cm wide, and 350 cm high. The experiment followed the principles of similarity theory. The geometric similarity ratio α_l was 100, and the other similarity coefficients satisfied Eqs. (1)–(3):

$$\alpha_t = \sqrt{\alpha_l}, \tag{1}$$

$$\alpha_\gamma = \frac{\gamma_p}{\gamma_m}, \tag{2}$$

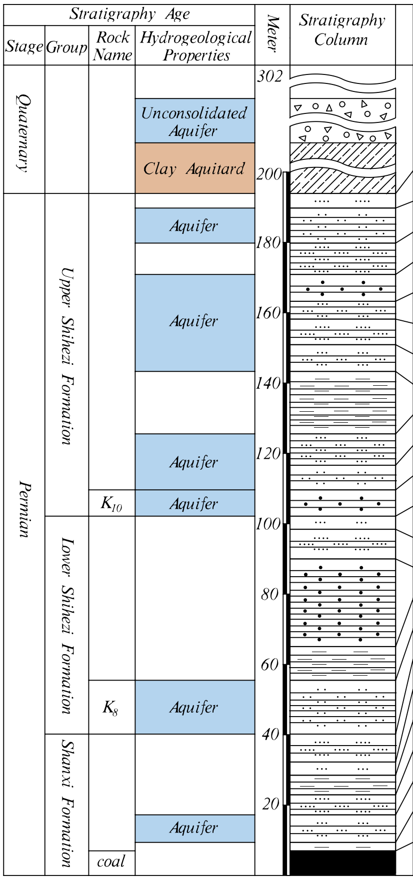

No.	Lithology	Thick m	Compression Strength Rc/MPa	Tensile Strength Rp/MPa	Natural Bulk Density γ /(kN • m⁻³)	Mixture ratio	Weight of similar material(kg)			
							river sand	lime	plaster	water
1	loess	108.10			16.6					
2	siltstone	4.15	33.53	3.08	20.7	355	68.91	11.49	11.49	10.21
3	medium grained sandstone	9.96	47.13	5.35	23.5	437	176.41	13.23	30.87	24.50
4	siltstone	8.92	38.43	4.36	21.6	355	148.12	24.69	24.69	21.94
5	coarse sandstone	7.62	35.12	3.86	26.7	355	126.53	21.09	21.09	18.75
6	fine grained sandstone	5.07	42.55	6.22	22.3	437	89.80	6.73	15.71	12.47
7	siltstone	7.27	40.53	5.31	21.3	355	120.72	20.12	20.12	17.88
8	fine grained sandstone	7.61	30.67	7.06	22.8	455	134.79	16.85	16.85	18.72
9	mudstone	17.75	21.13	0	24.1	537	327.49	19.65	45.85	43.67
10	fine grained sandstone	8.91	50.31	6.26	23.0	337	147.95	14.80	34.52	21.92
11	medium grained sandstone	7.01	46.67	6.23	24.5	337	116.40	11.64	27.16	17.24
12	coarse sandstone	7.47	43.57	3.18	27.3	437	132.31	9.92	23.15	18.38
13	fine grained sandstone	3.74	50.65	7.33	22.9	337	62.10	6.21	14.49	9.20
14	siltstone	8.42	55.82	3.41	21.2	973	167.78	13.05	5.59	20.71
15	coarse sandstone	24.92	75.12	5.88	26.5	955	496.56	27.59	27.59	61.30
16	mudstone	9.59	19.53	0	24.6	473	169.86	29.73	12.74	23.59
17	medium grained sandstone	15.30	60.23	4.77	23.3	973	304.87	23.71	10.16	37.64
18	siltstone	7.93	45.64	4.63	20.1	437	140.46	10.53	24.58	19.51
19	fine grained sandstone	3.77	52.56	6.75	22.9	337	62.60	6.26	14.61	9.27
20	mudstone	5.56	17.84	0	23.8	637	105.51	5.28	12.31	13.68
21	siltstone	5.69	58.65	5.73	21.1	973	113.38	8.82	3.78	14.00
22	fine grained sandstone	7.84	50.03	7.71	22.3	337	130.18	13.02	30.38	19.29
23	mudstone	2.40	29.21	0	24.2	455	42.51	5.31	5.31	5.90
24	No.3 coal seam	7.00	10.60	0	13.5	673	379.54	44.28	18.98	49.20

Fig. 2 A columnar lithostratigraphic cross section and the ratios of similar materials

$$\alpha_\sigma = \alpha_l \cdot \alpha_\gamma, \tag{3}$$

where α_t is the time ratio; α_γ is the bulk density ratio, which was 1.54 in this study; α_σ is the stress ratio, which was 154 in this study; γ_p is the bulk density of rock, which averaged 22.62 kN/m^3 in this study; and γ_m is the bulk density of the simulation materials, which averaged 14.70 kN/m^3. The simulated mining, with a cutting height of 7 cm and a speed of 10 cm/h, took 63.47 h.

According to rock physical mechanics, the research used: silica sand, river sand, and mica as the aggregates; lime and gypsum as the cementitious material; and borax at a concentration of 1.0% as a retardant. The mixture ratios and consumption of these materials were calculated using Eq. (4), as shown in Fig. 2:

$$G = lmh\gamma_m, \tag{4}$$

where G is the consumption of materials; l and m are the length and width of the model, respectively; h is the height of the layer; and γ_m is the bulk density of the simulation materials.

The strata were covered by a clay layer and an unconsolidated aquifer. The upper aquifer was in a floorless plexiglass box, which was inserted in the clay layer and covered with a Perspex plate to prevent evaporation.

Monitoring System

A set of monitoring points at 20 cm intervals both horizontally and vertically was attached to the strata from the seam roof to the clay layer floor, for a total of 10 rows, 21 columns, and 215 monitoring points. Overburden displacements were recorded using XTDP photography (optics) measurement systems.

The fractures that developed during and after extraction were recorded by a digital camera, and the fracture statistics were determined using the "image rectification" and "attribute analysis" functions of MAPGIS software (V6.7, Zondy cyber, Wuhan, Hubei, China).

For easier water level observation, a glass tube with two open ends and scales was pasted vertically on the box. After the clay aquitard was saturated, the water tables were measured bihourly to obtain the pre-mining seepage velocity. If the water level drop exceeded 1 cm, water was added to the tank to maintain a constant head. During mining, the water level was measured every 2 h. If a large flux and fast seepage were encountered later in the excavation, the frequency of observations were increased.

Numerical Simulation

A numerical groundwater flow model was constructed using the MODFLOW code in GMS (Groundwater Modeling System), which is a well-known three-dimensional finite-difference groundwater flow model (Kallioras et al. 2010; Martin and Frind 1998; Mohammadzadeh et al. 2017).

Hydrogeological Conceptual Model

Groundwater flow in an unconsolidated aquifer was modeled. A relatively integrated hydrogeological unit was selected as the simulation area, which extended westward and northward to the water divide and was bounded to the east and south by the Zhuozhang South Yuan and Jiang Rivers, respectively (Fig. 3). The modeled area was ≈ 22.4 km from east to west and 10.4 km from north to south, and covered ≈ 232.4 km^2. In profile, the phreatic surface is the top boundary, and the no. 3 coal seam floor is the bottom boundary. Based the field investigation and 135 stratigraphic logs from throughout the area, the model thickness ranged from 241 to 872.34 m with a mean of 556.67 m, and the strata were generally inclined from west to east and north to south. Flow occurs through porous media, which included two main types in the study area: an unconsolidated aquifer in the Quaternary and a fissured aquifer in the Permian clastic rocks. The unconsolidated aquifer basically consists of a sand and gravel complex in the Middle (Q_2) and Lower Pleistocene (Q_1). The silty clay underlying the unconsolidated aquifer is regarded as an aquitard because of its weak permeability and low water yield property. The water-bearing system included nine layers from top to bottom: a phreatic aquifer in the Middle Pleistocene strata, a relative aquitard, a confined aquifer in the Lower Pleistocene strata (target aquifer), a silty clay aquitard (target aquitard), a confined aquifer within the bedrock fissure of sandstone in the Permian strata (P_2s, P_1x, P_1s), the coal seam and the floor.

The study area is a complex multilayer aquifer system. Groundwater flow in the unconsolidated aquifer obeys Darcy's law. The Jiang River is a partially penetrating river due to shallow channel incision, while the Zhangze reservoir has a deep incision. The partially penetrating wells and mine drainage give the groundwater a vertical velocity, so the groundwater flow is characterized by three-dimensionality. The percolation media are heterogeneous since the hydrogeological parameter varies with lithology. In addition, the

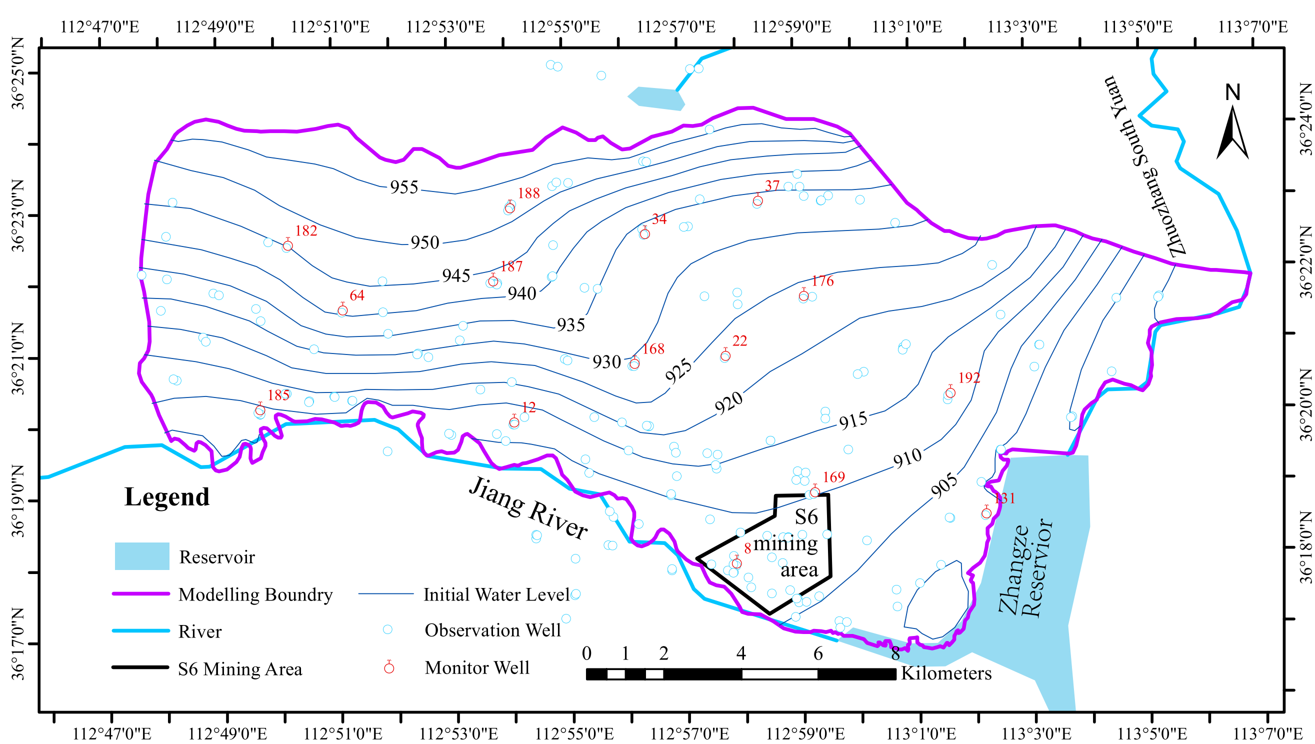

Fig. 3 Simulation area

parameters change over time and the underground water flow changes spatially, so the groundwater had an unsteady flow. To summarize, the groundwater flow model system can be generalized into three-dimensional isotropic heterogeneous and unsteady flows.

Model Setup and Structure

The mathematical model of groundwater is as follows:

$$\frac{\partial}{\partial x}\left(K\frac{\partial H}{\partial x}\right)+\frac{\partial}{\partial y}\left(K\frac{\partial H}{\partial y}\right)+\frac{\partial}{\partial z}\left(K\frac{\partial H}{\partial z}\right)+W = S_s\frac{\partial H}{\partial t}\ (x,y,z)\in D, t\geq 0, \tag{5}$$

$$H(x,y,z,0)=H_0(x,y,z)\ (x,y,z)\in D, \tag{6}$$

$$H(x,y,z,t)=f(x,y,z,t)\ \ (x,y,z)\in D, \tag{7}$$

$$K\frac{\partial H}{\partial n}\bigg|_{S_2}=q(x,y,z,t)\ \ (x,y,z)\in S_2, \tag{8}$$

where D is the flow area (m^2); K is the hydraulic conductivity (m/day); H is hydraulic head of point (x,y,z) at time t (m); Ss is the specific storage (dimensionless); H_0 is the groundwater level elevation at time t = 0 (m); f is the river level (m); W is the volume flux per unit volume representing a source/sink (m/day); $\vec{n}$ is the normal vector of the boundary; q is the inflow or outflow volume flux from a unit area at a unit time of the second type boundary (m^3/day), where the inflow is positive and the outflow is negative; and S_2 is the second boundary.

Spatial discretization: Based on the interrelations among the mesh density, model accuracy and computational load (Tok and Il 2018), the model was implemented horizontally through a 100 × 100 m grid and was divided vertically into 2–7 layers per formation. Considering that there were fractures in the damaged zone, the meshes surrounding the mining area were refined, and the layers in the fractured water-conducting zone were also refined to conduct hydraulic conductivity divisions. The grid was composed of 307 rows, 165 columns, and 23 layers. The cells outside the model area were marked as inactive cells; the effective cells totaled 282,576, representing a 232.3 km^2 area (Fig. 4).

Temporal discretization: based on data from 203 observation wells and a groundwater level survey, a complete hydrological year, from July 2015 to June 2016 was selected as the simulation period. The water level observed in July 2015 was chosen as the initial water level.

Boundary condition: The northern boundary of the model domain was the surface and shallow groundwater divide, which was considered to be the second type boundary conditions. The tributaries were flux boundaries (recharge boundaries) and the others were no-flow type. The eastern and southern boundaries were outflow boundaries and were considered to be the general head boundary condition. The western boundary was roughly parallel to the general groundwater flow direction, which can be treated as the no-flow type. Vertically, the saturated zone was recharged by precipitation, irrigation infiltration, and lateral flow from the mountain tributaries (La Licata et al. 2018), and the upper boundary was defined as the flux boundary. The coal seam floor was the relative water-resisting strata, so the lower boundary was treated as a no-flux boundary.

Parameter determination: Hydraulic conductivity and specific storage are the two most important hydrogeological parameters for simulating groundwater dynamics (Brandyk et al. 2016; Qiu et al. 2015; Tok and Il 2018). The hydraulic parameters were obtained from borehole pumping test results and geological exploration reports. The coefficients of the precipitation infiltration and the return flow of irrigation were identified by Parameter Estimation, and the inversion results within the range of experience values from the handbook of hydrogeology were available. According to the lithology and water yield properties of the porous media, the parameters were divided into seven zones (Supplemental Figure S-1 and Supplemental Table S-1).

The source/sink terms: The lateral boundary was evaluated depending on the properties and scale of each boundary and then applied into the model using the Special Flow Package. The groundwater recharge mainly originated from the infiltration of precipitation, the canal system, returning irrigation water, and flow from tributaries along the northern boundary. A 2D file was generated for the returning irrigation water and infiltration of precipitation as areal recharge and then imported into the Recharge Package. The groundwater discharge was dominated by drainage into the river and reservoir and artificial pumping for industrial, agricultural, and domestic use. In the southern area, the groundwater discharged into the deep valley and recharged the river or the Quaternary unconsolidated pore water. River runoff discharge was calculated by the Specified Head Package. The groundwater withdrawal was classified into concentrated and areal exploitations, the domestic wells and industrial wells belonged to concentrated pumping and were calculated by the Well Package, and the agricultural irrigation belonged to the areal exploitation, which was represented by 2D files.

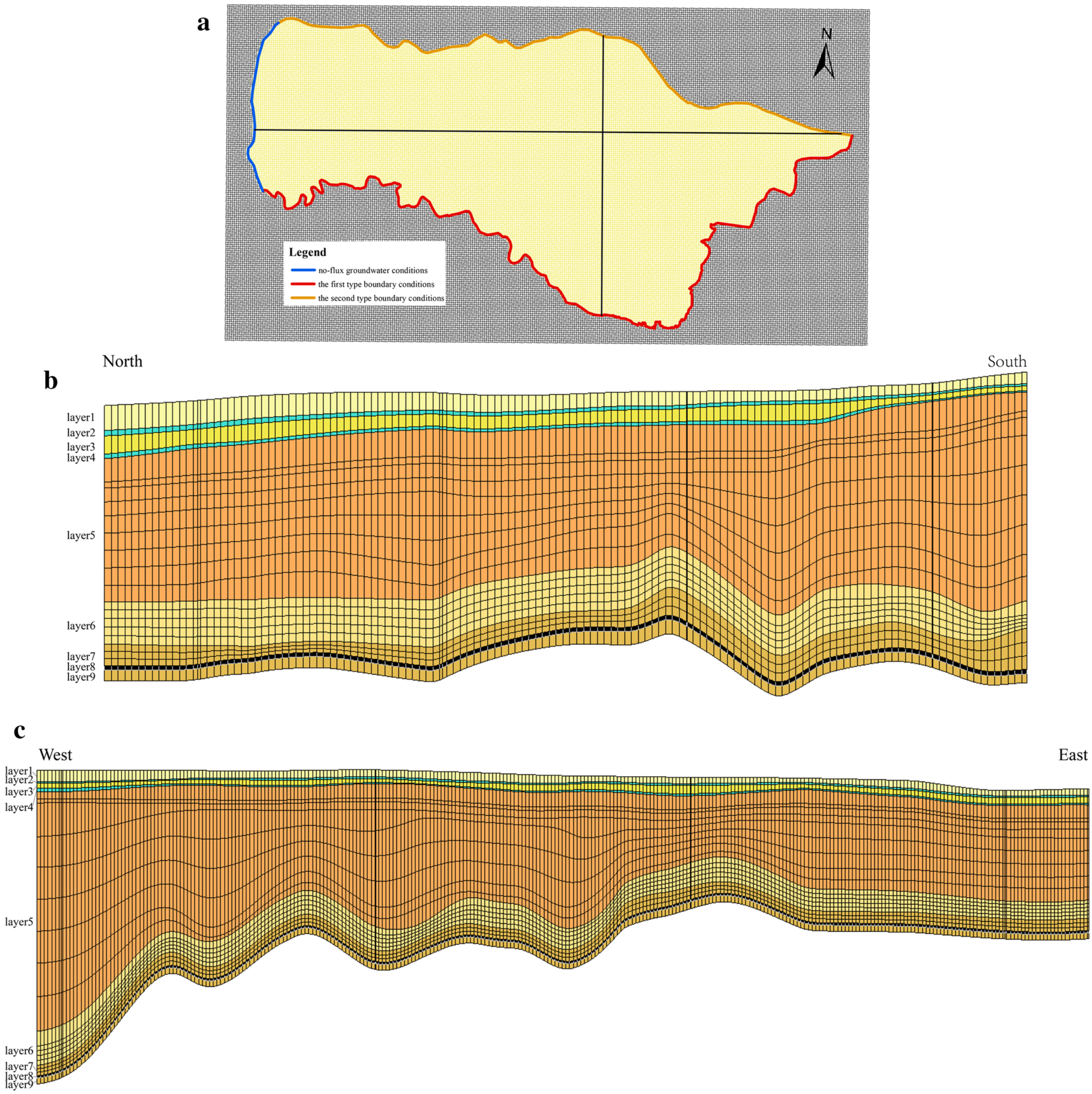

Fig. 4 Spatial discretization **a** horizontal (in the figure, black lines indicate the section traces), **b** vertical in N–S, **c** vertical in W–E

Model Calibration and Validation

Based on field surveys and simultaneous groundwater level measurement of in July 2015, the starting heads of each node (grid point) in the Quaternary unconsolidated porous aquifer were obtained by the Inverse Distance Weighted interpolation. The initial flow field was determined by analyzing the hydrogeological conditions.

The water level monitoring data from 2015 to 2016 from 15 monitoring wells evenly distributed throughout the modeled area were used to calibrate the parameters and validate the model. The distribution of the monitoring wells is shown in Fig. 3. The model calibration and validation were carried out for the period of Jul. 9th to Oct. 12th, 2015 and Oct. 13th, 2015 to Jul. 4th, 2016, respectively. The calibration period lasts 96 days and was uniformly divided into 12 phrases, with 8 days in each phrase; the validation period lasts 266 days and was divided into 14 phrases. After the parameters were repeatedly adjusted, the calculated water levels matched the measured values well, and the fitting errors were within the permissible error limits (Supplemental Figure S-2 and Supplemental Table S-2).

Prediction Scheme

The validated model was applied to calculate the groundwater levels for the assumed parameters of the aquitard and to quantitatively estimate the potential impact on the unconsolidated aquifer. Two predictive scenarios can be obtained relative to aquitard properties changes. The groundwater flow dynamic variation was quantitatively simulated by adjusting the: (1) aquitard thickness (M), which was set at 10, 20, 40, 60, or 80 m, and (2) hydraulic conductivity of the aquitard (K), which was set at 10^{-3}, 7.39×10^{-5}, 10^{-5}, 10^{-6}, or 10^{-7} cm/s.

The simulations assumed that the groundwater in the Permian bedrock fissure aquifer had dropped to the coal seam floor. Based on the verified model and considering the large permeability variation in the fractured water-conducting zone, the changed hydraulic conductivities were set to the fracture zone (Supplemental Figure S-3). The values were divided into three zones according to the characteristics of the fracture distribution (Zhang et al. 2018). The water inflow at an average of 180 m^3/h was spread evenly over the S6 mining area and drained through the wells (Sun et al. 2015; Xie et al. 2018). In this study, the area with a drawdown larger than 2 m was treated as the affected area.

Results and Discussion

Physical Modeling Results

Following coal extraction, deformation and movement were generated, and fractures formed in the overburden strata (Fig. 5). The maximum height of the interconnected fractures was approximately 145.4 m, which was 20 times the mining height, and was located 61.5 m from the unconsolidated aquifer. The result conforms to the results obtained from the adjacent regional site measurements.

The clay layer beneath the unconsolidated aquifer overlies the bedrock, and its deformation was determined by rock mass movement (Huang 2014). Measured data from horizontal monitoring lines H_9 and H_{10} show that subsidence and deformation of the aquitard occurred despite its remoteness from the fractured zone. After mining, significant subsidence of the clay layer appeared near the mine void space; the maximum subsidence was 4.8 m. The overburden with displacements exceeded 300 m in width, which was wider than the excavated scope and accordant with the site observations. In addition, tensile stress occurring in the strata subsidence process caused tension fractures to appear on the surface around the gob.

Variation in the mean seepage velocity of groundwater over time under pre- and post-mining conditions is shown in Fig. 6. The seepage velocity before mining was 0.0278 cm/h. As the coal was mined, the infiltration was relatively stable until the mining approached 200 m, leaking at a constant speed of 0.0278 cm/h on average, which matched the pre-mining conditions, showing that the unconsolidated aquifer was not affected. Subsequently, the water level declined dramatically, and the seepage velocity increased to 0.0977 cm/h when the digging was complete. Thus, although the fractured water-conducting zone (damaged strata) had not propagated to the aquifer, groundwater seepage increased. The unconsolidated aquifer was affected by mining disturbance.

A degree of deformation can lead to damaged structures and fractures as well as degraded stability (Fan and Zhang 2015; Xu et al. 2018). The probable reason for the increasing seepage velocity is that the clay aquitard tensile deformed continually during mining; when the mining advanced to 200 m, the aquitard fissured and the porosity increased. Thereafter, the impermeability of the aquitard was weakened, and the effective thickness of the water-resisting layer thinned, which accelerated groundwater leakage. Therefore, the unconsolidated aquifer suffered substantial damage.

The water loss that indirectly resulted from mining was slow but continuous. The leakage from the upper unconsolidated aquifer should not be ignored, although it does not influence mining safety. The aquitard's properties play a crucial role in groundwater depletion: the leakage varies directly with its permeability and inversely with the path length.

Numerical Simulation Results

The water level in the unconsolidated porous aquifer dropped, and the permeability and effective thickness of the aquitard were the main reasons for this decrease. The response of the groundwater level in an unconsolidated aquifer to mining was studied for two scenarios:

Scenario 1: The hydraulic conductivity of the clay layer was constant ($K=7.39\times10^{-5}$ cm/s), the thicknesses were 10, 20, 40, 60, or 80 m, respectively. The affected area and drawdown of the Quaternary unconsolidated aquifer at 1, 3, and 5 years after mining are shown in Fig. 7.

The thickness of the aquitard beneath the unconsolidated aquifer markedly affects the groundwater flow regime. The thicker the aquitard, the more advantageous it was for water storage and the longer the groundwater leakage path was, resulting in a smaller influential area and less water loss. When the thickness of the aquitard was greater than or equal to 40 m, the aquitard had a high water-resistance. The drawdown was less than 3 m and showed no significant change with thickness, even while the impacted range decreased progressively with increasing thickness of the clay layer. This

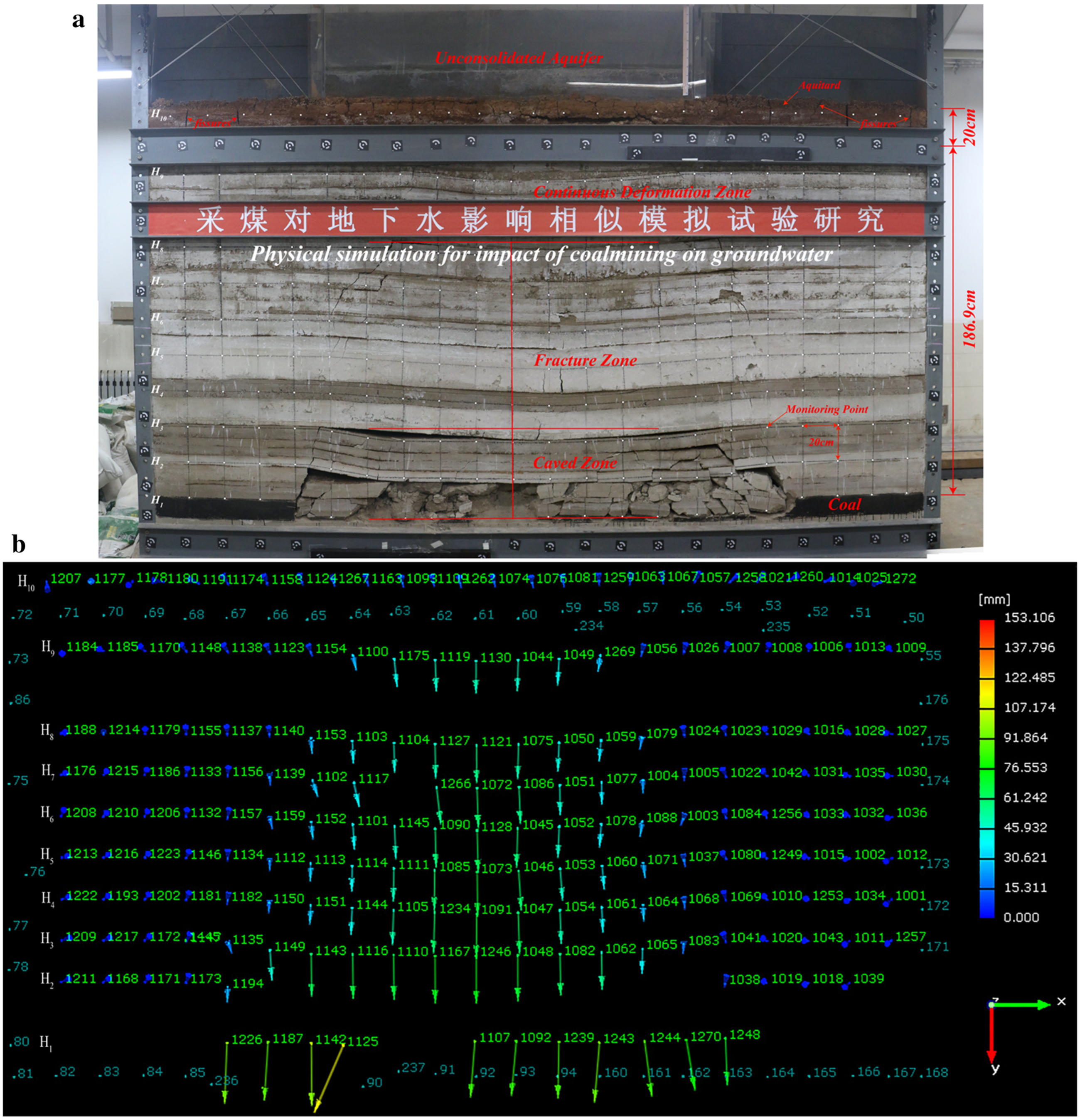

Fig. 5 The deformation and fractures in the aquitard **a** deformation and fractures, **b** subsidence

result occurred because the porous aquifer mainly received lateral recharge, and the vertical recharge was limited. From the perspective of time, the drawdown and influential area changed dramatically during the first year of mining. Three years after mining, the groundwater inflow and outflow were generally at equilibrium; the affected scope and drawdown were basically unchanged or changed slightly with time when the aquitard was 40 m or higher. Furthermore, following the decrease in the aquitard thickness, the maximum drawdown was greatly increased and was less likely to achieve a steady state over time. Compared with the mining influence on the aquifer under the actual geological setting, where the affected area was 46.1 km^2 and the maximum drawdown was 10.02 m after mining was completed, a 40 m thick clay layer could effectively prevent the leakage of groundwater. The groundwater levels and drawdown contour map of the unconsolidated aquifer at this point are shown in Fig. 8. It can be observed that the affected scope

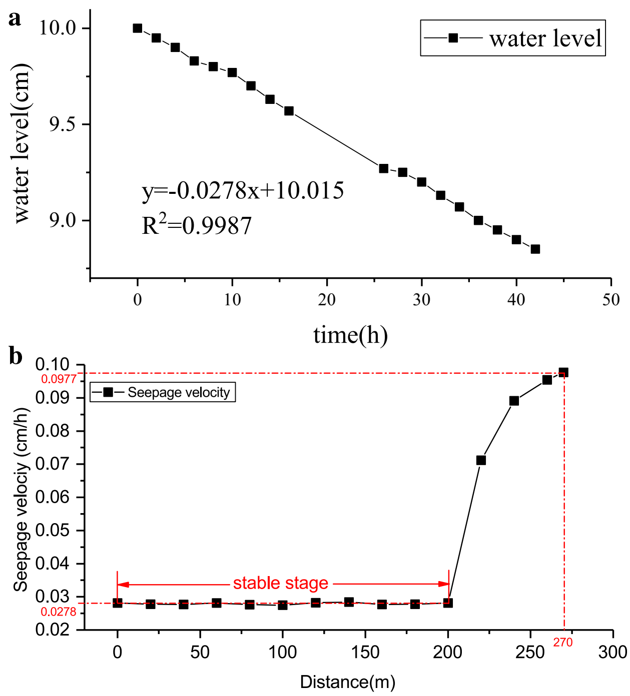

Fig. 6 Variation in the mean seepage velocity **a** premining, **b** post-mining

was limited to the mining and nearby areas, and that the maximum drawdown was 2.93 m.

Scenario 2: The thickness of the clay layer was held constant (M = 20 m), and the hydraulic conductivities were set at 10^{-3}, 7.39×10^{-5}, 10^{-5}, 10^{-6}, and 10^{-7} cm/s. The affected area and drawdown of the Quaternary unconsolidated aquifer at 1, 3, and 5 years after mining are shown in Fig. 9.

The increased hydraulic conductivity of the aquitard floor expanded the cone of depression and increased the aquifer drawdown, which could seriously affect groundwater resources (Fig. 9). When the hydraulic conductivity was increased to 10^{-3} cm/s, the influenced area could reach 54 km^2 in 5 years, with a drawdown of 13 m, even if the porous aquifer was far from the damaged strata. The influence range of the unconsolidated aquifer changed dramatically during the first year of mining but subsequently changed less. The maximum drawdown changed little when the hydraulic conductivity was less than 10^{-6} cm/s; the drawdown and affected area could reach a basically stable state after 3 years of mining. Compared to the mining influence on the aquifer under actual geological settings after 5 years of mining, a clay layer of 10^{-6} cm/s in hydraulic conductivity could effectively prevent the leakage of groundwater. The groundwater levels and drawdown contour map of the unconsolidated aquifer at this point are shown in Fig. 10.

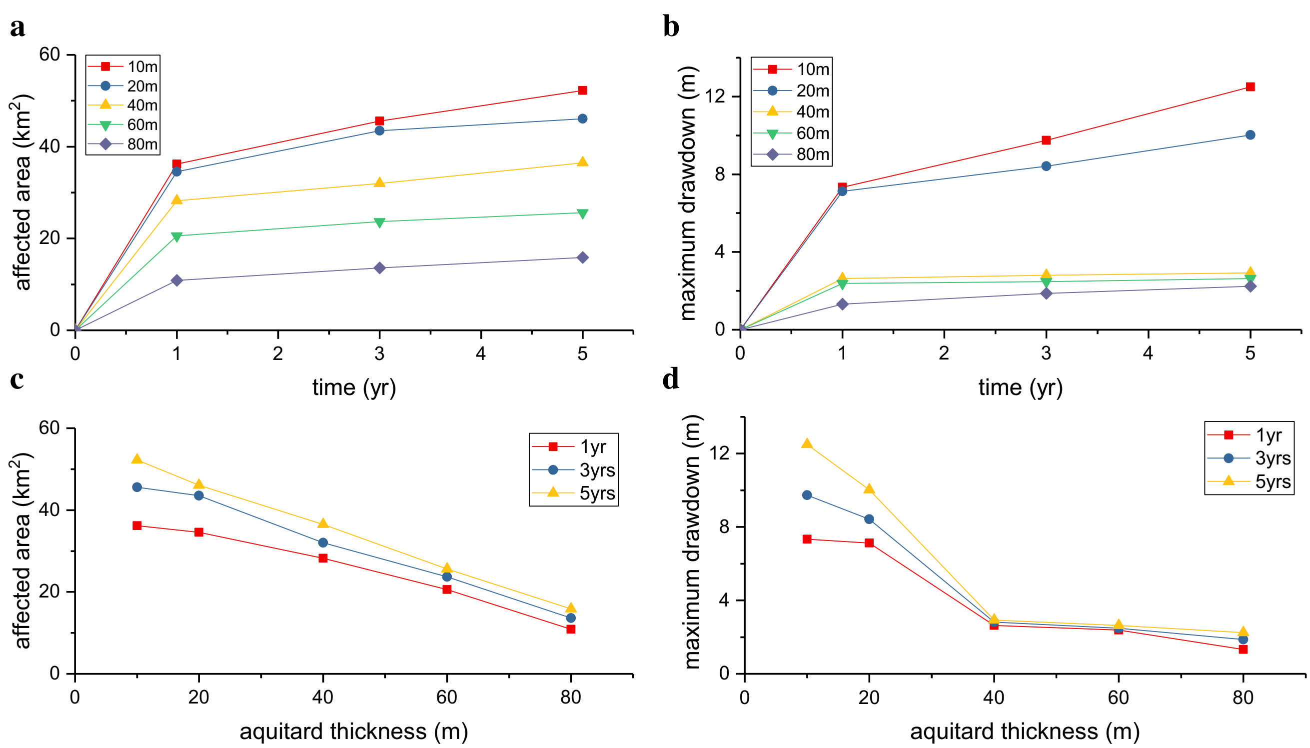

Fig. 7 The mining influence on the aquifer with the thickness of the aquitard over time **a** the affected area with time, **b** the maximum drawdown with time, **c** the affected area with thickness, **d** the maximum drawdown with thickness

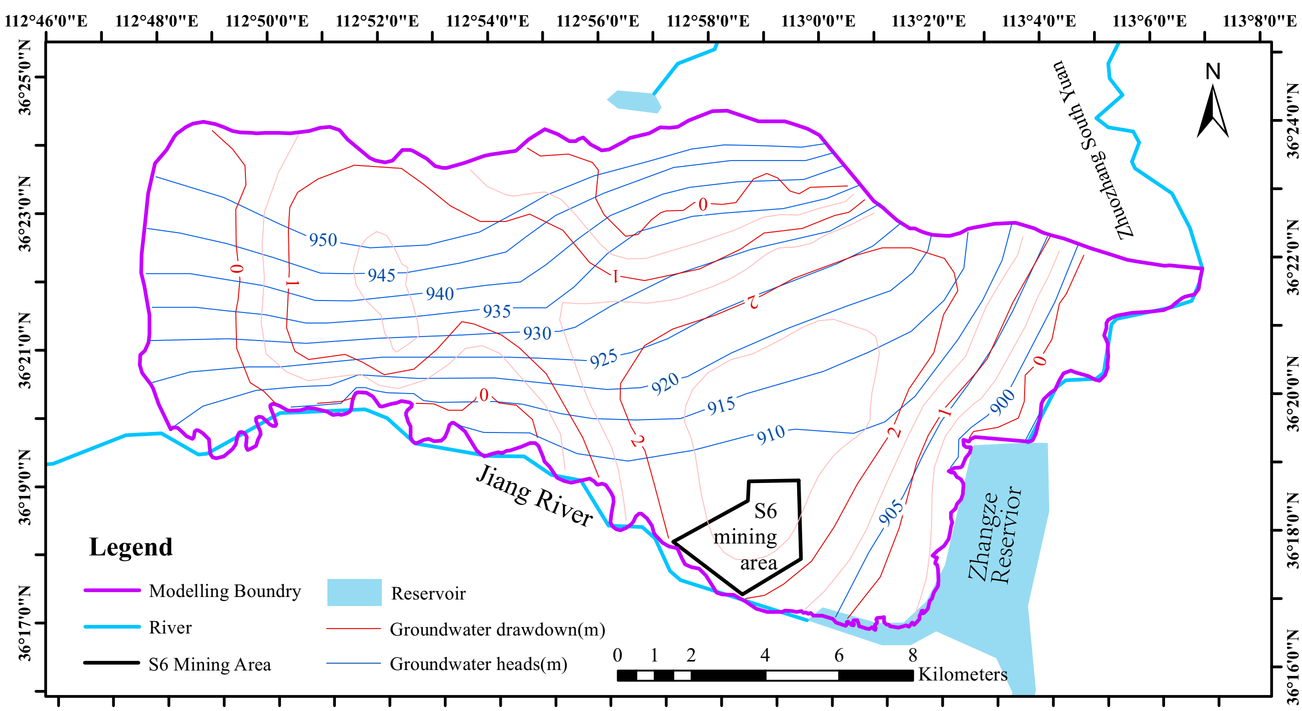

Fig. 8 The groundwater levels and drawdown contour map of the unconsolidated aquifer after 5 years of mining at the K = 7.39 × 10^{-5} cm/s and M = 40 m

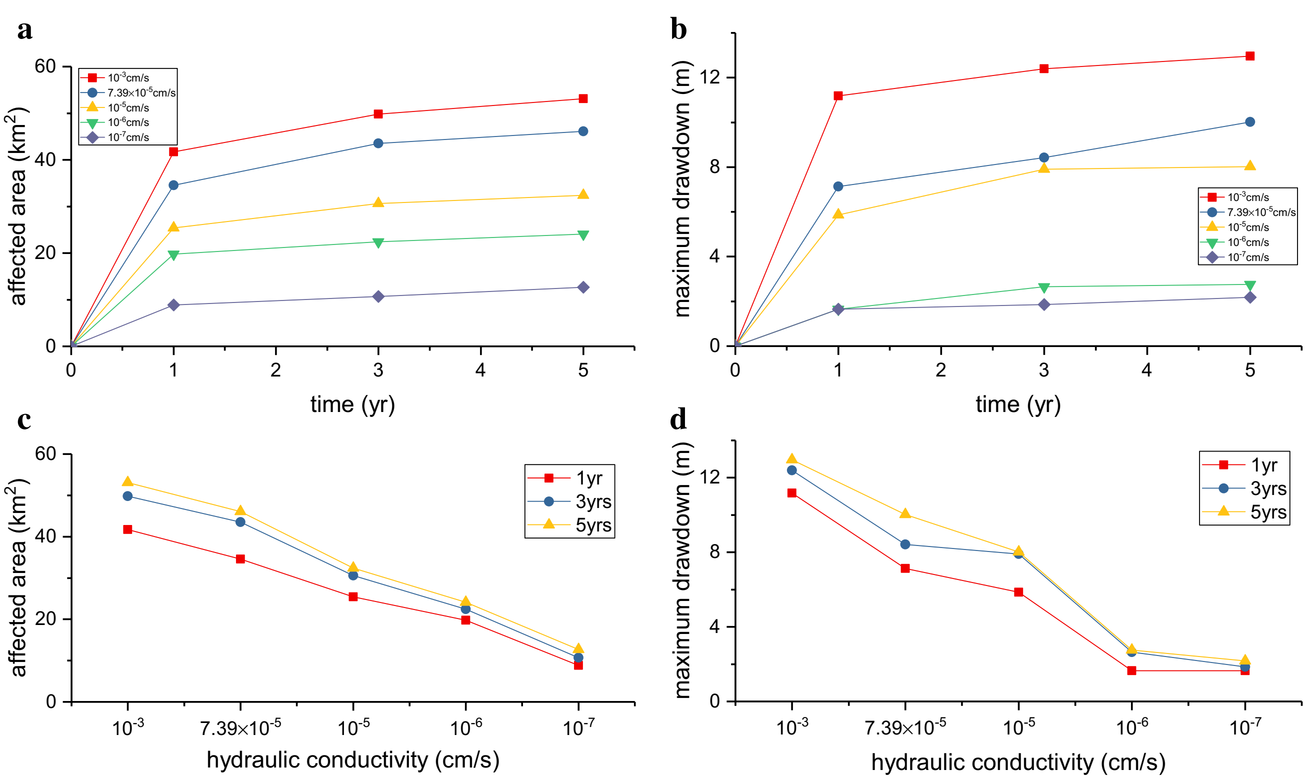

Fig. 9 The mining influence on the aquifer with the hydraulic conductivity of aquitard over time **a** the affected area with time, **b** the maximum drawdown with time, **c** the affected area with hydraulic conductivity, **d** the maximum drawdown with hydraulic conductivity

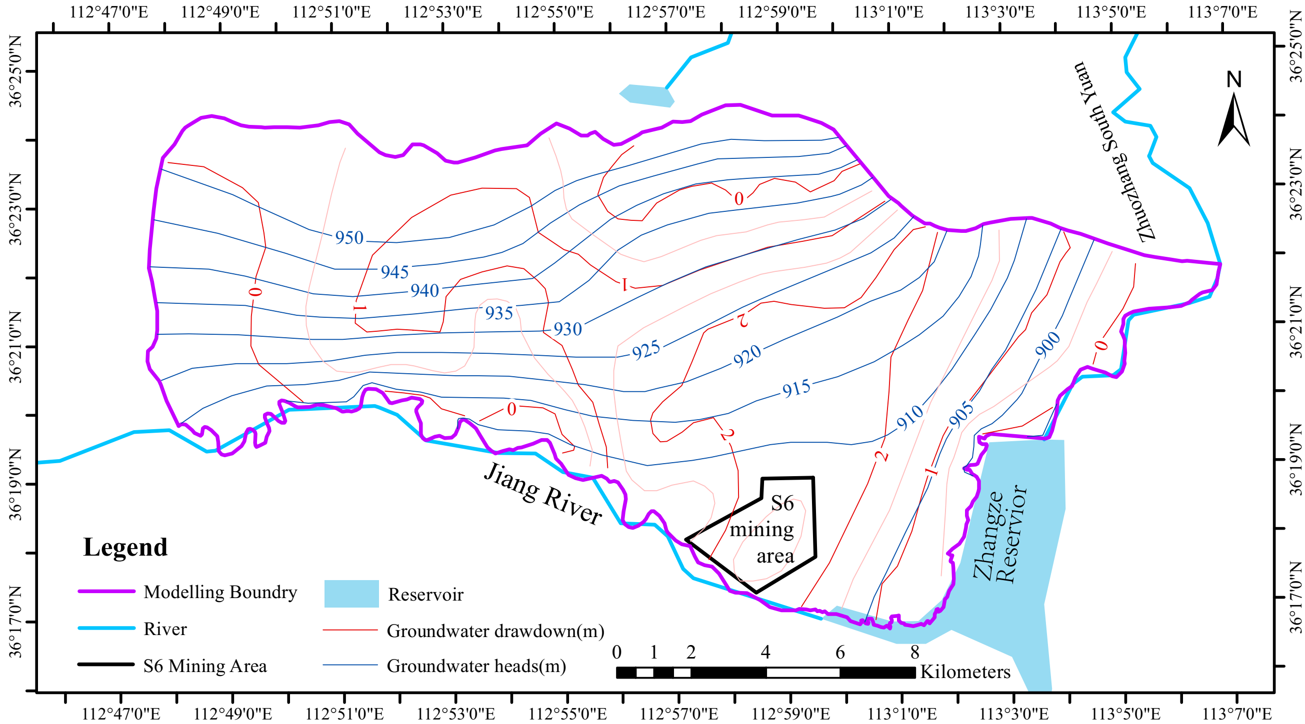

Fig. 10 The groundwater levels and drawdown contour map of the unconsolidated aquifer after 5 years of mining at the M = 20 m and K = 10^{-6} cm/s

Note that the maximum drawdown was 2.76 m, which could be followed by recovery.

Discussion

Two ways to consider the drawdown follow. First, although the rock mass and clay aquitard in the continuous bending zone were not severely damaged, the deformation caused fissures and provided a pathway along which groundwater could flow into the downward cracks and accumulate at the distal end. Then, the deep saturated soil along the fissure plane was permeated, and the cracks further expanded. Thus, the penetrability of the clay floor was increased even further. The seepage process was generally observed in the clayey layer. Another reason that the permeability increased was that the original water storage structure and the hydrophysical properties of the silty clay were influenced by compression and shearing in the stress redistribution process, so that the groundwater in the unconsolidated aquifer penetrated consistently and increasingly through the silty clay. This change in the impermeability was the critical reason for the loss of water in the unconsolidated aquifer. Next, the sequential disturbances to the overlying rock layers in the deep mining area led the flow of the bedrock fissure water to mostly permeate vertically. The groundwater in the bedrock fissures of the aquifers drained to the working face, and the head difference between the upper and lower aquifers increased continuously. The groundwater in the overlying Quaternary unconsolidated aquifer did not flow directly into the gob but instead leaked and recharged the dewatered fissured aquifer through the aquitard because of the difference in water pressure. Then, the water level of the Quaternary unconsolidated aquifer decreased. In short, the increased hydraulic gradient, along with a decrease in the impermeability of the aquitard, led to continuous groundwater leakage.

This study's numerical simulations focused on the flow from a leaky aquifer and considered the changes in the permeability of the damaged rock. The impacts of the aquitard properties on groundwater flow were predicted and analyzed from the perspective of water protection. Decreasing the hydraulic conductivities by an order of magnitude and doubling the thickness of the clay can both be efficiently implemented to preserve water during mining.

Conclusion

Physical and numerical simulations were used to indicate the impacts of aquitard properties on an overlying unconsolidated aquifer in a coal mining area of the Loess Plateau. Based on the results of the physical simulation, the failure characteristics and hydrogeological variations in the aquifer after coal mining are reflected mainly by deformation and subsidence, which produce fractures of the aquitard floor, resulting in increased permeability as well as water level drops. Underground mining affected unconsolidated aquifers in two ways: by decreasing the impermeability of the aquitard, and by increasing the hydraulic gradient between the porous aquifer and fractured bedrock aquifers. The influential degree depends primarily on the properties of the clay layer, in which the impermeability improves with increased thickness or decreased hydraulic conductivity. A thinner aquitard and higher permeability reduces water resistance, leading to the unconsolidated aquifer being more easily affected, with a greater and more widespread impact. The response of the groundwater level to coal extraction was predicted in a porous aquifer under different hydraulic conductivities and aquitard thicknesses using the finite-difference method. The maximum drawdown changed slightly when the hydraulic conductivity was less than 10^{-6} cm/s and the aquitard thickness was greater than 40 m.

These results can aid in better understanding the mechanisms by which underground mining can influence an overlying unconsolidated aquifer outside the disturbance failure zone and the groundwater flow response to the overburden damaged in porous media. Moreover, they can serve as a theoretical basis for water conservation during mining and coal industry sustainable development in the semiarid Chinese Loess Plateau. The clay aquitard is thick or impermeable enough to prevent groundwater loss, and thus, grouting an aquitard in dense fissures zones could be helpful for the coal industry and ecoenvironmental protection.

Acknowledgements This research was funded by the National Natural Science Foundation of China, Grant 41572221; Research Fund of Key Research Program of Ministry of Science and Technology for Water Resources Efficient Development and Utilization Project [2018YFC0406403]; and the National Natural Youth Science Foundation of China, grant 41502243. We gratefully acknowledge the financial support and thank Engineers Haodong Sun and Xue Wang and Assistant researcher Jun Zhu for aiding in conducting this research. We also thank the editors and peer reviewers for their time, careful work, and helpful suggestions.

References

Ben-Itzhak LL, Gvirtzman H (2005) Groundwater flow along and across structural folding: an example from the Judean Desert, Israel. J Hydrol (Amsterdam) 312(1–4):51–69

Bian Z, Miao X, Lei S, Chen S, Wang W, Struthers S (2012) The challenges of reusing mining and mineral-processing wastes. Science 337(6095):702–703

Booth CJ (2006) Groundwater as an environmental constraint of longwall coal mining. Environ Geol 49(6):796–803

Brandyk A, Majewski G, Kiczko A, Boczoń A, Wróbel M, Porretta-Tomaszewska P (2016) Ground water modelling for the restoration of Carex communities on a sandy river terrace. Sustainability 8(12):1324

Du F, Gao R (2017) Development patterns of fractured water-conducting zones in longwall mining of thick coal seams—a case study on safe mining under the Zhuozhang River. Energies 10(11):1856

Fan G, Zhang D (2015) Mechanisms of aquifer protection in underground coal mining. Mine Water Environ 34(1):95–104

Hill JG, Price DR (1983) The impact of deep mining on an overlying aquifer in western Pennsylvania. Groundwater Monit Remediat 3:138–143

Huang Q (2014) Research on cracks zone of clay aquiclude in overburden. Appl Mech Mater 548–549:1744–1747

Izady A, Abdalla O, Joodavi A, Chen M (2017) Groundwater modeling and sustainability of a transboundary hardrock–alluvium aquifer in North Oman Mountains. Water 9(3):161

Kallioras A, Pliakas F, Diamantis I (2010) Simulation of groundwater flow in a sedimentary aquifer system subjected to overexploitation. Water Air Soil Pollut 211(1–4):177–201

Karacan CÖ, Goodman G (2009) Hydraulic conductivity changes and influencing factors in longwall overburden determined by slug tests in gob gas ventholes. Int J Rock Mech Min Sci 46(7):1162–1174

Kloosterman FH, Stuurman RJ, Meijden RVD (1995) Groundwater flow systems analysis on a regional and nation-wide scale in the Netherlands: the use of flow systems analysis in wetland management. Water Sci Technol 31(8):375–378

La Licata I, Colombo L, Francani V, Alberti L (2018) Hydrogeological study of the glacial—fluvioglacial territory of Grandate (Como, Italy) and stochastical modeling of groundwater rising. Appl Sci 8(9):1456

Liu J, Elsworth D, Matetic RJ (1997) Evaluation of the post-mining groundwater regime following longwall mining. Hydrol Process 11(15):1945–1961

Ma L, Jin Z, Liang J, Sun H, Zhang D, Li P (2015) Simulation of water resource loss in short-distance coal seams disturbed by repeated mining. Environ Earth Sci 74(7):5653–5662

Martin PJ, Frind EG (1998) Modeling a complex multi-aquifer system: the Waterloo moraine. Groundwater 36(4):679–690

Miao X, Cui X, Wang J, Xu J (2011) The height of fractured water-conducting zone in undermined rock strata. Eng Geol 120(1–4):32–39

Mohammadzadeh H, Dadgar MA, Nassery H (2017) Prediction of the effect of water supplying from Shirindare dam on the Bojnourd aquifer using Modflow 2000. Water Resour 44(2):216–225

Newman C, Agioutantis Z, Leon GBJ (2017) Assessment of potential impacts to surface and subsurface water bodies due to longwall mining. Int J Min Sci Tech 27(1):57–64

Peng SS (1992) Surface subsidence engineering. Soc for Mining, Metallurgy and Exploration, New York City

Qiu S, Liang X, Xiao C, Huang H, Fang Z, Lv F (2015) Numerical simulation of groundwater flow in a river valley basin in Jilin urban area, China. Water 7(10):5768–5787

Scanlon BR, Keese KE, Flint AL, Flint LE, Gaye CB, Michael Edmunds W, Simmers Ian (2010) Global synthesis of groundwater recharge in semiarid and arid regions. Hydrol Process 20(15):3335–3370

Singh MM, Kendorski FS (1981) Strata disturbance prediction for mining beneath surface water and waste impoundments. In: Proc, 1st conf on ground control in mining, West Virginia Univ, Morgantown

Sun W, Wu Q, Liu H, Jiao J (2015) Prediction and assessment of the disturbances of the coal mining in Kailuan to karst groundwater system. Phys Chem Earth Parts A/B/C 89–90:136–144

Tammetta P (2015) Estimation of the change in hydraulic conductivity above mined longwall panels. Groundwater 53(1):122–129

Tok GC, Il JK (2018) Method of simulation and estimation of SCW system considering hydrogeological conditions of aquifer. Energy Build 163(15):140–148

Wang M, Li J (1987) Technology of mine water control in China. Mine Water Environ 6(3):25–38

Xie P, Li W, Yang D, Jiao J (2018) Hydrogeological model for groundwater prediction in the Shennan mining area, China. Mine Water Environ 37(3):505–517

Xu S, Zhang Y, Shi H, Wang K, Geng Y, Chen J (2018) Physical simulation of strata failure and its impact on overlying unconsolidated aquifer at various mining depths. Water 10(5):650

Yang Y, Kalin R, Zhang Y, Lin X, Zou L (2001) Multi-objective optimization for sustainable groundwater resource management in a semiarid catchment. Hydrol Sci J 46(1):55–72

Yuan H, Zhang G, Yang G (2009) Numerical simulation of dewatering thick unconsolidated aquifers for safety of underground coal mining. Int J Min Sci Technol 19(3):312–316

Zeng Y, Wu Q, Liu S, Zhai Y, Lian H, Zhang W (2018) Evaluation of a coal seam roof water inrush: case study in the Wangjialing coal mine, China. Mine Water Environ 37(1):174–184

Zhang D, Fan G, Ma L, Wang X (2011) Aquifer protection during longwall mining of shallow coal seams: a case study in the Shendong Coalfield of China. Int J Coal Geol 86(2–3):190–196

Zhang S, Tang S, Zhang D, Fan G, Wang Z (2017) Determination of the height of the water-conducting fractured zone in difficult geological structures: a case study in Zhao Gu no. 1 coal seam. Sustainability 9(7):1077

Zhang Y, Xu Y, Wang K, Chen P, Wang X, Zheng Q, Zhang Z (2018) The fracturing characteristics of rock mass of coal mining and its effect on overlying unconsolidated aquifer in Shanxi, China. Arab J Geosci 11:666